Earth Planet. Sci. Lett. 643 (2024) 118897

Contents lists available at ScienceDirect

Earth and Planetary Science Letters

journal homepage: www.elsevier.com/locate/epsl

Revisiting zircon Eu anomaly as a proxy for crustal thickness: A case study of the Sierra Nevada Batholith

Ming Tang [a,*], Ziyi Guo [a], Wenrong Cao [b], Xu Chu [c]

[a] Key Laboratory of Orogenic Belt and Crustal Evolution, MOE; School of Earth and Space Sciences, Peking University, Beijing 100871, PR China
[b] Department of Geological Sciences and Engineering, University of Nevada, Reno, MS-172, 1664 N. Virginia St., Reno, NV 89557, USA
[c] Department of Earth Sciences, University of Toronto, 22 Russell Street, Toronto, Ontario M5S 3B1, Canada

ARTICLE INFO

Keywords:
Zircon Eu/Eu*
Crustal thickness
Sierra Nevada Batholith
La/Yb

ABSTRACT

We analyzed detrital zircon from the Sierra Nevada Batholith, western USA, to reassess whether zircon Eu/Eu* can be used to reconstruct crustal thickness in the past. Our reconstruction shows two episodes of crustal thickening between 80–200 Ma in the Sierra Nevada region—one during the Jurassic (170—140 Ma) and the other in the Cretaceous (110—80 Ma). These findings are consistent with the results obtained using the whole-rock La/Yb proxy and observations on crustal deformation. Our results underscore the validity of zircon Eu/Eu* proxy for tracing the evolution of crustal thickness at the batholith or orogen scale, provided that a sufficient number of analyses are obtained. Recent petrologic models questioned the validity of the zircon Eu/Eu* proxy because of the complex interplay among various factors that may affect zircon Eu/Eu*. These models, however, overlooked the interconnections between these factors. In particular, magma redox condition and water content, which are known to significantly impact zircon Eu/Eu*, may also be controlled by differentiation pressure and thus crustal thickness. Therefore, rather than complicating the interpretation, these factors could potentially enhance the pressure control on zircon Eu/Eu*.

1. Introduction

Quantifying the evolution of crustal thickness holds significant importance in unraveling the complex interplay among tectonism, magmatism, and climate in orogens (Lee et al., 2015). However, the thickness of crust as it is preserved today may not accurately reflect past conditions due to processes such as erosion, gravitational collapse, and lower crust recycling. To address this challenge, several geochemical proxies based on magma compositions have been proposed (Chapman et al., 2015; Chiaradia, 2015; Haschke et al., 2002; Profeta et al., 2015). Tang et al. (2021b) extended this approach to zircon and showed that the Eu anomaly (Eu/Eu* = chondrite normalized Eu/sqrt(Sm*Gd)) in zircon correlates with the La/Yb ratio of felsic magmas, thus providing insights into the thickness of the crust at the time of active magmatism. This new proxy opens the avenues for reconstructing crustal thickness in magmatically active regions using the extensive detrital zircon archives.

The relationship between zircon Eu/Eu* and crustal thickness is based on empirical observations and reflects pressure-sensitive mineral fractionation through either fractional crystallization or partial melting. Europium occurs as Eu^{2+} and Eu^{3+} in most magmatic systems (Weill and Drake, 1973). As magmatic differentiation occurs at low pressures in a thin crust, plagioclase is a major fractionating mineral that preferentially depletes Eu^{2+} in the melt (Ren, 2004), imprinting a low Eu/Eu* signature in the melt and zircon. Conversely, in a thick crust, magmatic differentiation pressure is systematically higher and suppresses plagioclase saturation, mitigating the Eu depletion in zircon. Additionally, at high pressures, Eu partitioning in zircon is further enhanced due to endogenic oxidation effect associated with garnet fractionation (Tang et al., 2018; Tang et al., 2019; Tang et al., 2020). Because garnet prefers Fe^{2+} relative to Fe^{3+} under crustal melting temperature conditions (Holycross and Cottrell, 2023), garnet fractionation preferentially removes Fe^{2+} from the melt and oxidizes Eu^{2+} to Eu^{3+}, which is more compatible in zircon than Eu^{2+} (Burnham and Berry, 2012; Trail et al., 2012).

The initial assessment of the zircon Eu/Eu* proxy was conducted in a single magmatic orogen—Gangdese magmatic orogens in southern Tibet. Since its proposal, the zircon Eu/Eu* proxy has been applied in various local and global contexts (e.g., Brudner et al., 2022; Chen et al., 2022; Sundell et al., 2022; Tang et al., 2021a). However, the validity of this proxy for indicating crustal thickness has been contested by phase

* Corresponding author.
E-mail address: mingtang@pku.edu.cn (M. Tang).

https://doi.org/10.1016/j.epsl.2024.118897
Received 24 March 2024; Received in revised form 7 July 2024; Accepted 13 July 2024
Available online 21 July 2024

equilibria and geochemical modeling results (e.g., Triantafyllou et al., 2023; Yakymchuk et al., 2023). The major concern on the validity of this proxy is that zircon Eu/Eu* can be influenced by multiple variables that may not be easily constrained (Roberts et al., 2024). For example, Yakymchuk et al. (2023) conducted a series of phase equilibria modeling experiments coupled with trace element partitioning calculations. They showed that pressure, oxygen fugacity, source composition, and temperature/differentiation degree all contribute to zircon Eu/Eu* variability. Additionally, Triantafyllou et al. (2023) emphasized the role of magma water content, which affects the stability of garnet and plagioclase, on zircon Eu/Eu* based on similar modeling experiments.

Here, we re-examine the reliability of this proxy through a case study on the Sierra Nevada batholith in western North America. We will compare our reconstructed crustal thickness using Eu/Eu* in detrital zircon with previous estimates based on whole-rock La/Yb ratio and additional geologic evidence, and discuss their implications for the tectonic evolution of the Sierra Nevada. We will then discuss why the current phase equilibria and geochemical modeling yielded results that contrast with observations. Finally, we will evaluate the potential and limitations of zircon Eu/Eu* as a proxy for crustal thickness.

2. Geologic background and samples

The North America continent witnessed accretions of island arcs and exotic terranes onto its western margin in the Paleozoic and Mesozoic. From Early-Middle Triassic to Late Cretaceous, magmatic arcs were developed along the western margin of North America as a consequence of the eastward subduction of the Farallon plate (Dickinson, 2004). The Sierra Nevada arc, one of the arc segments, is now exposed as the Sierra Nevada Batholith (SNB) in California. The predominant lithologies of the SNB include tonalites, granodiorites, and granites. Less differentiated, including intermediate and mafic rocks, are sporadically distributed in the batholith. The Sierra Nevada magmatism is characterized by a cyclic style, with flare-ups occurring at ~ 220, 160, and 100 Ma in the central Sierra according to igneous and detrital zircon records (Paterson and Ducea, 2015).

The general compression of the Sierra Nevada arc was punctuated by episodic regional extension. From the Early-Middle Triassic to Middle Jurassic, arc-perpendicular extension was evidenced by shallow marine sedimentation that now crop out as batholith pendants (Attia et al., 2021; Busby-Spera, 1988). The subsequent arc-perpendicular shortening in the Late Jurassic, previously recognized as the Nevadan Orogeny, was attributed to the accretion of off-shore terranes and island arcs (Saleeby et al., 2015; Schweickert et al., 2015). Since ~150 Ma, the western margin of the North America was consolidated as a coherent arc-trench system, when the Sierra Nevada arc was predominantly subject to compression evidenced by the intra-arc shortening (Cao et al., 2015) and Sevier fold-thrust belt in the retro-arc and foreland regions (DeCelles, 2004). At ~ 90 Ma, arc magmatism migrated inland due to the Laramide flat subduction (e.g., Yonkee and Weil, 2015).

Plate subduction and arc/terrane accretion led to an interplay of magmatism and crustal thickening in the Sierra Nevada region (Cao and

Fig. 1. Map showing river sand sampling sites and drainage areas in the Sierra Nevada region.

Paterson, 2016; Cao et al., 2016; Lewis et al., 2023; Profeta et al., 2015), making it an ideal location to test detrital zircon Eu/Eu* a proxy for reconstructing crustal thickness. We collected modern river sands from eight tributaries whose drainage basins cover the central and southern Sierra Nevada batholith as well as the beach of Lake Tahoe (Fig. 1, Table 1). To mitigate the impact of damming that filters river sands, we specifically targeted upper stream areas for sampling.

3. Methods

Zircon grains were separated from the river sands, mounted, and polished before being analyzed for their U-Pb isotopes and trace elements simultaneously at Beijing Quick-Thermo Science & Technology Co., Ltd. The measurements were done using an Agilent 8900 inductively coupled plasma triple-quadrupole mass spectrometer (ICP-QQQ-MS) connected to an ESI New Wave NWR 193UC (TwoVol2) laser ablation system. We followed analytical procedures similar to those outlined in Ji et al. (2020). Laser ablation was conducted in a continuous helium carrier gas stream mixed downstream with nitrogen and argon before entering the torch region of the ICP. Oxide production rate measured as $^{232}Th^{16}O^{+}/^{232}Th^{+}$ ratio was maintained at ≤0.2 %. U/Th fractionation measured as $^{238}U^{+}/^{232}Th^{+}$ ratio during NIST SRM 610 ablation was tuned to 0.95–1.05 in line scanning mode.

All analyses were conducted in spot mode, with a 30 µm diameter beam size, ~4 J/cm^2 energy, and 5 Hz repetition rate. Each analysis comprised a 30 s signal collection, involving 10 s on background (laser off) and 20 s on zircon (laser on). Background subtraction and correction for laser downhole elemental fractionation for the time-resolved LA-ICP-MS data were executed using the Iolite data reduction package within the Wavemetrics Igor Pro data analysis software (Paton et al., 2010). The detailed dataset is provided in Supplementary File 2.

For U-Pb age calibration, zircon 91500 served as the external reference material. Zircon SA01 was routinely measured as an unknown to monitor instrument performance. For trace element concentration calibration, NIST610 glass was used as the external reference material, with Si serving as the internal standard. Zircon 91500 and NIST610 were measured twice before and after 6–8 sample analyses. Repeated analyses of SA01 have mean $^{206}Pb/^{238}U$ age and Eu/Eu* values of 535.9 ± 1.5 Ma (2 SE) and 1.15 ± 0.15 (2 SD), respectively (Figs. S1 and S2). These measured age and Eu/Eu* values are consistent with the recommended values of 535.08 ± 0.32 Ma (2 SD, CA-ID-TIMS result) and 1.15 ± 0.12 (2 SD), respectively (Huang et al., 2019).

4. Results

4.1. Geochronology

We measured a total of 2694 detrital zircon grains that were randomly selected from the nine sand samples (~300 grains for each sand sample). The $^{206}Pb/^{238}U$ age distribution of each sample is plotted in Fig. 2. Among the dated grains, ~97 % are of Mesozoic ages. The bulk age distribution shows two prominent peaks at ~100 Ma and ~160 Ma (Fig. 3B). These peaks, individually or combined, are also noticeable in each sample (Fig. 2), aligning with two magmatic flare-ups in the Jurassic and Cretaceous (DeCelles et al., 2009; Paterson and Ducea, 2015). Arc magmatism appears to have ceased by ~80 Ma (Fig. 3B), which is likely associated with the influence of flat-slab subduction (Saleeby et al., 2003).

Table 1
River sand sample sites

Sample ID	River	Longtitude	Latitude
23NB-4-1	Lake Tahoe	−119.9534	38.9803
23SN-1-MKL	Mokelumne River	−120.7201	38.3129
23SN-2-MED	Mecred River	−119.9650	37.6070
Sanj23_CRN_01	San Joaquin River	−119.3379	37.2195
KINGS23_CRN_01	Kings River	−119.1309	36.8707
MFK22_CRN_03S	Kawean River	−118.9118	36.4340
23SN-4-TUL	Tule River (middle fork)	−118.8159	36.1300
23SN-5-KEN-NK	Kern River (north fork)	−118.4221	35.7553
23SN-6-KEN-SK	Kern River (south fork)	−118.2899	35.6728

4.2. Trace elements and reconstructed crustal thickness

We applied specific criteria, as outlined in Table 2, to filter the trace element data. These criteria were used to eliminate data compromised by mineral inclusions, metamorphic alteration, zircon grains originating from S-type granites and co-crystallizing with titanite. These filtering procedures reduce the dataset by ~27 %, leaving us with 1958 data points.

We then used these data to calculate crustal thickness utilizing the empirical correlation between zircon Eu/Eu* and crustal thickness established by Tang et al. (2021b). The data were binned into 2 Myr intervals. It is worth noting that intervals with fewer than 10 data points exhibit significant variability in mean crustal thicknesses, warranting caution in interpreting results of particular bins. Overall, our data show a substantial fluctuation in crustal thickness between 200–80 Ma in the Sierra Nevada region (Fig. 3A). This variation highlights two episodes of crustal thickening—during the Jurassic (170—140 Ma) and the Cretaceous (110—80 Ma)—each coinciding with magmatic flare-ups in the Sierra Nevada region (Fig. 3B).

5. Discussion

5.1. Comparison with La/Yb proxy results and geologic observations

The La/Yb ratio of andesitic and felsic magmas has been widely used to constrain crustal thickness (e.g., Farner and Lee, 2017; Haschke et al., 2002; Lieu and Stern, 2019; Profeta et al., 2015; Zhu et al., 2017). The La/Yb ratio was also used to quantify crustal thickness in the calibration of the zircon Eu/Eu* proxy (Tang et al., 2021b). Briefly, the rationale of the La/Yb proxy is that crustal thickening changes the mineral phases in equilibrium with evolved melts from plagioclase + pyroxene ± olivine at low pressures, to plagioclase + amphibole ± pyroxene at medium pressures, and to garnet + pyroxene ± amphibole at high pressures (Chen et al., 2023; Green, 1982). This change in the mineralogy of the crystallizing assemblage leads to progressively fractionated La/Yb ratio in the melt, making La/Yb ratio a sensitive indicator of differentiation pressure/crustal thickness (Farner and Lee, 2017; Profeta et al., 2015).

We first compare the crustal thickness reconstructed using detrital zircon and whole-rock data, which represent two independent records of crustal evolution. Our zircon results provide a decent data coverage for the Jurassic through Cretaceous time, with more than 10 zircon analyses available for each 2 Myr interval across the majority of the timeframe. For time intervals with > 10 zircon analyses, our reconstruction of crustal thickness using Eu/Eu* ratios in detrital zircon aligns well with estimates derived from the whole-rock La/Yb proxy, and both proxies consistently record two major crustal thickening episodes (Fig. 3A). We note that, for the Jurassic time period, crustal thicknesses estimated from zircon Eu/Eu* appear slightly greater than those calculated from whole-rock La/Yb. However, these discrepancies fall within the range of uncertainty and are generally smaller than 5–10 km. In addition, slight differences in the calculated crustal thickness may also arise from the different sampling biases of the detrital zircon and whole-rock records.

In intervals with < 10 zircon analyses, such as between 190–180 Ma and 140–130 Ma, the estimates of crustal thickness derived from zircon Eu/Eu* show greater variability and significant deviations from the results obtained from whole-rock La/Yb. We attribute these discrepancies to inadequate analyses of detrital zircon (and probably also whole rock samples) because zircon, even within a single pluton, records a spectrum of Eu/Eu* due to continuous plagioclase co-crystallization. Note that these variations in melt and zircon Eu/Eu* are temporal and

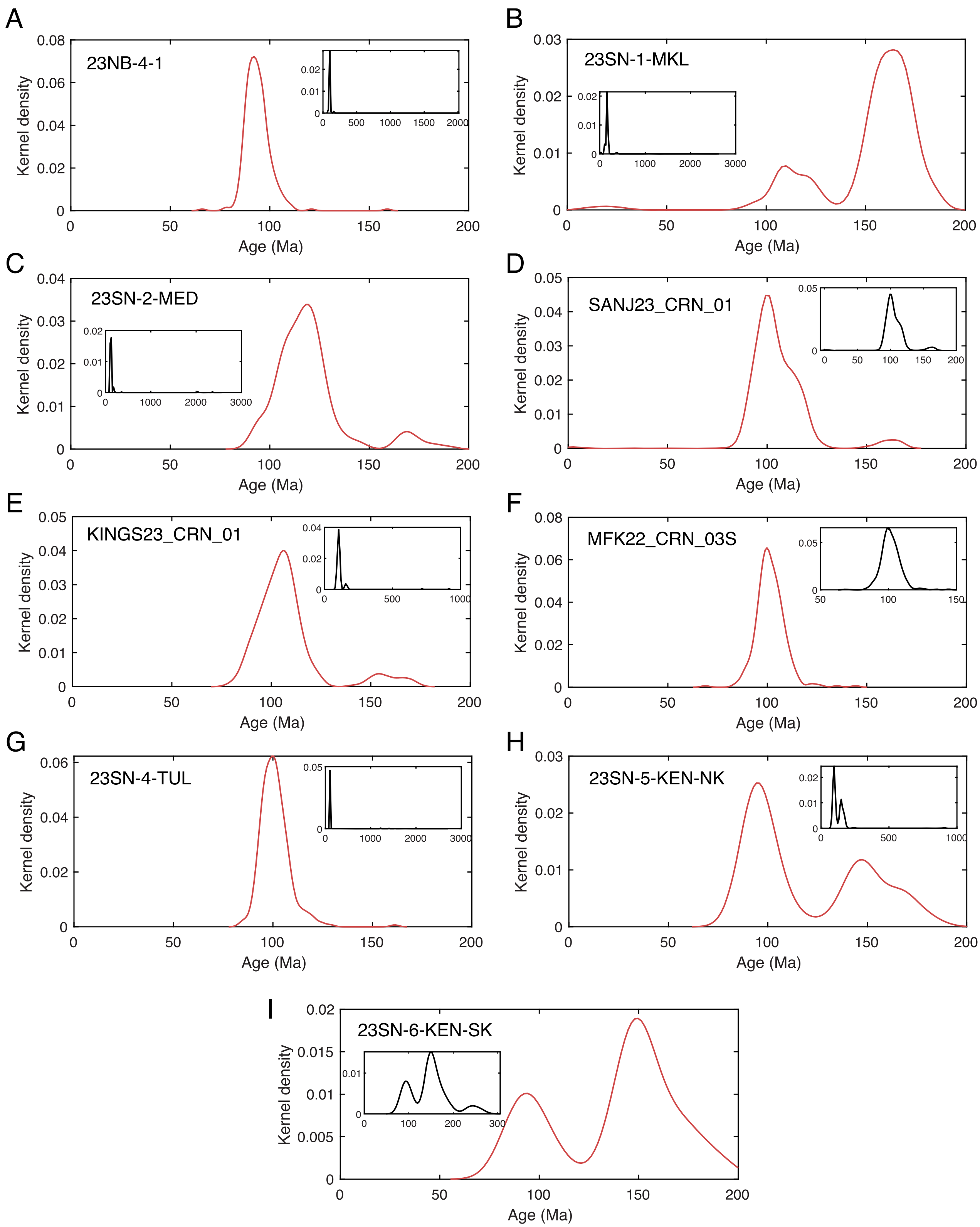

Fig. 2. Kernel density plots of $^{206}Pb/^{238}U$ age of detrital zircon grains separated from the sand samples collected in the Sierra Nevada batholith. Each panel includes an inset displaying the complete distribution.

not necessarily spatial (Tang et al., 2024b). Therefore, a reliable estimate of crustal thickness can only be achieved by the mean Eu/Eu* ratio from a sufficiently large number of zircon analysis (Tang et al., 2021b).

Two significant crustal thickening events occurred in the Middle-Late Jurassic (~170–150 Ma) and Middle-Late Cretaceous (~110–80 Ma). These thickening episodes are supported by several lines of geologic evidence. Firstly, both episodes temporally match with the peaks of retro-arc and intra-arc shortening (Fig. 3E and F). Furthermore, these episodes coincide with magmatic flare-ups (Fig. 3B), indicating an important role for magmatic addition in driving crustal thickening in the

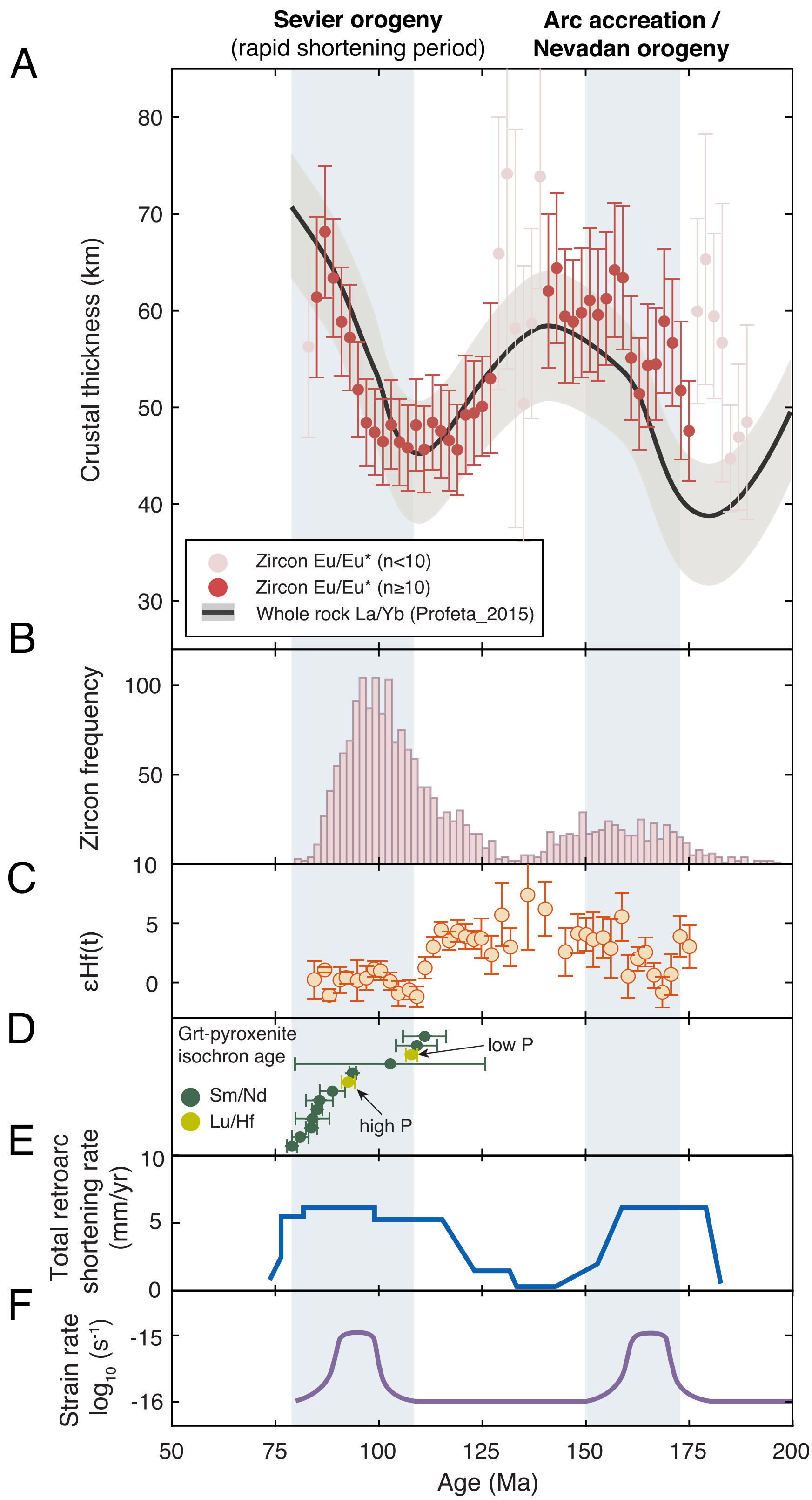

Fig. 3. A. Crustal thickness evolution of the Sierra Nevada batholith reconstructed using Eu/ Eu* in detrital zircon. The data are plotted as binned averages (bin size = 2 Myr) and 2 SE errors. For each bin, we removed 10 % of the data with the highest values and 10 % with the lowest values to minimize the influence of outliers. The dark curve bracketed by a gray band shows the average crustal thickness, with 2 SE margins, calculated from La/Yb ratio of felsic rocks within the Sierra Nevada batholith (Profeta et al., 2015). B. Age distribution of detrital zircon analyzed in this study. C. Evolution of Hf isotopes of the Sierra Nevada batholith compiled by Cao et al. (2022). D. Mineral Sm/Nd and Lu/Hf isochron ages of garnet pyroxenite cumulates in the Sierra Nevada region (Chin et al., 2015; Ducea and Saleeby, 1998b). E. Total retro-arc shortening rate (Yonkee and Weil, 2015). F. Intra-arc strain rate estimated by Cao et al. (2015).

Table 2
Zircon trace element data filters

Filter	Removal criteria	Data remaining (%)	Notes
La concentration	> 1 ppm	2527/2694 (93.8 %)	Analyses with high La concentrations are likely compromised by inclusions (Tang et al., 2021b).
Th/U ratio	< 0.1	2520/2694 (93.5 %)	Analyses with low Th/U may reflect zircon of metamorphic origins (Hoskin and Schaltegger, 2003).
Ta concentration	< 0.2 ppm	2013/2694 (74.8 %)	Analyses with low Ta concentrations may indicate significant titanite co-crystallization, which may cause high Eu/Eu* in zircon (Loader et al., 2017).
P concentration	> 750 ppm	1985/2694 (73.7 %)	High-P zircon may come from S-type granites (Burnham and Berry, 2017)
Eu/Eu*	> 1	1960/2694 (72.7 %)	Affected by feldspar inclusions?

Sierra Nevada region (Cao and Paterson, 2016; Cao et al., 2016). Secondly, the mineral Sm/Nd and Lu/Hf isochron ages of garnet-pyroxenite cumulates, which formed by deep magmatic differentiation at pressures exceeding 1 GPa (Rapp and Watson, 1995; Wolf and Wyllie, 1993), also point to substantial crust thickening between 110–80 Ma (Chin et al., 2015; Ducea and Saleeby, 1998a; Ducea and Saleeby, 1998b). Thirdly, hot metasedimentary quartzites with zircon lower intercept U-Pb ages of 103 ± 10 Ma also suggest intense underthrusting of retro-arc crust in the Sierra Nevada region during the Middle Cretaceous (Chin et al., 2013).

Between the two thickening events, crustal thickness shows a decreasing trend from 150 to 110 Ma, which is somewhat puzzling considering the lack of signs of extension during this period. This thinning event witnesses a ~15 km crustal thickness reduction over ~40 Myr, coinciding with a magmatic lull (Fig. 3B), reduced shortening rates in retro-arc and intra-arc settings (Fig. 3E and F), and juvenile isotopic signatures (Fig. 3C). While the exact geologic mechanism is beyond the scope of this study, we speculate that this thinning event from the Late Jurassic to Early Cretaceous might be related to the foundering of the Jurassic arc root as proposed by DeCelles et al. (2009). DeCelles et al.'s model emphasizes cyclicity in the evolution of Cordilleran orogenic systems, positing that the combination of high magmatic flux and underthrusting of retro-arc crust leads to the thickened arc crust and dense arc roots. The dense arc root could impede mantle flow, ultimately leading to the cessation of magmatism. Arc magmatism resumes as dense arc root delaminates, which in turn reinstates mantle flow. We propose that the Jurassic to Cretaceous crustal thickening and thinning pattern could reflect one such cyclic process. The magmatic lull may have been a consequence of arc root formation during the Jurassic magmatic flare-up and crustal thickening. The subsequent root foundering may have paved the way for another cycle of magmatic flare-up and crustal thickening by the Middle Cretaceous.

5.2. Implications for reconstructing crustal thickness evolution using zircon Eu/Eu*

Several recent studies have raised questions regarding the validity of zircon Eu/Eu* as a proxy for reconstructing the evolution of crustal thickness (e.g., Triantafyllou et al., 2023; Yakymchuk et al., 2023). However, this case study of the Sierra Nevada batholith presented here and that of the Gangdese batholith (Tang et al., 2021b) serve to underscore the potential of zircon Eu/Eu* as a valuable tool for this purpose, at least in Phanerozoic continental arcs. The skepticism of Triantafyllou et al. (2023) and Yakymchuk et al. (2023) were drawn from phase equilibria and geochemical modeling, pointing out that Eu/Eu* in zircon is controlled by not only differentiation pressure/crustal thickness, but also by redox conditions, magma water content, differentiation, and source compositions. We discuss below the influences of these factors and the limitations of the zircon Eu/Eu* proxy.

5.2.1. Redox

Redox equilibrium between Eu^{3+} and Eu^{2+} impacts the Eu/Eu* ratio in the melt and zircon through two primary mechanisms. Firstly, because Eu^{2+} is less compatible than Eu^{3+} in zircon (Burnham and Berry, 2012; Trail et al., 2012), oxidation enhances Eu partitioning in zircon. Thus, zircon crystallizing from oxidized melts tends to have higher Eu/Eu*. Secondly, under oxidized conditions, the depletion of Eu by plagioclase crystallization is attenuated since Eu^{3+} is much less compatible than Eu^{2+} in plagioclase (Ren, 2004). Therefore, oxidized melts will exhibit higher Eu/Eu* than reduced melts when they are in equilibrium with the same amount of plagioclase. This in turn translates into higher Eu/Eu* in zircon. Both mechanisms collectively contribute to an increase in Eu/Eu* ratio in zircon under oxidized conditions. If redox condition was considered as an independent variable (Triantafyllou et al., 2023; Yakymchuk et al., 2023), the lack of constraint on redox condition could indeed complicate the interpretation of zircon Eu/Eu*.

However, it is important to note that the redox condition may be also strongly associated with differentiation pressure, particularly in the context of felsic magmas derived from basaltic protoliths. At high pressures (> 1 GPa) as garnet becomes stabilized as a residual phase, the $Fe^{3+}/\sum Fe$ increases in the melt (Tang et al., 2018; Tang et al., 2019), so felsic magmas generated beneath thickened crust are intrinsically oxidized (see Holycross and Cottrell (2023) and Tang et al. (2024c) for a recent debate on this hypothesis). By contrast, felsic magmas formed at low pressures would be inherently reduced due to the fractionation of magnetite that has a high $Fe^{3+}/\sum Fe$. Sun and Lee (2022) modeled this influence of pressure on redox condition and showed that increasing differentiation pressure can potentially lead to >4 orders of magnitude increase in fO_2.

Several recent studies suggested that, similar to garnet, amphibole crystallization may also elevate $Fe^{3+}/\Sigma Fe$ in the derivative melt and cause oxidation (Luo et al., 2024; Zhang et al., 2022). However, we note that the endogenic oxidation effect associated with amphibole crystallization is weak (< 1 log units increase in fO_2 after extensive amphibole fractionation, Luo et al. (2024)) and only becomes significant when the magma already attains a high melt $Fe^{3+}/\Sigma Fe$ of > 0.2–0.3 (Zhang et al., 2022). The weak oxidation effect of amphibole crystallization is likely due to the high Fe^{3+} compatibility and $Fe^{3+}/\Sigma Fe$ in amphibole (Goltz et al., 2022; Zhang et al., 2022). As an arc crust thickens, the change in fractionating phases from being plagioclase-bearing to being amphibole- and plagioclase-bearing, and finally to being clinopyroxene- and garnet-bearing may lead to a gradual increase in the endogenic oxidation effect (and magma La/Yb ratio) with crustal thickening, which progressively increases Eu compatibility in zircon.

Collectively, endogenic oxidation process, if occurring, would link the redox condition of felsic magmas to differentiation pressure/crustal thickness. To further evaluate this co-evolution hypothesis, we apply the zircon Ce-Ti-U oxybarometer (Loucks et al., 2020) to our detrital zircon dataset to quantify the fO_2 of the Sierra Nevada batholith through time. As shown in Fig. 4, the trend of fO_2 closely follows that of crustal thickness. In particular, the two major crustal thickening periods are both accompanied by significant magma oxidation. This consistency

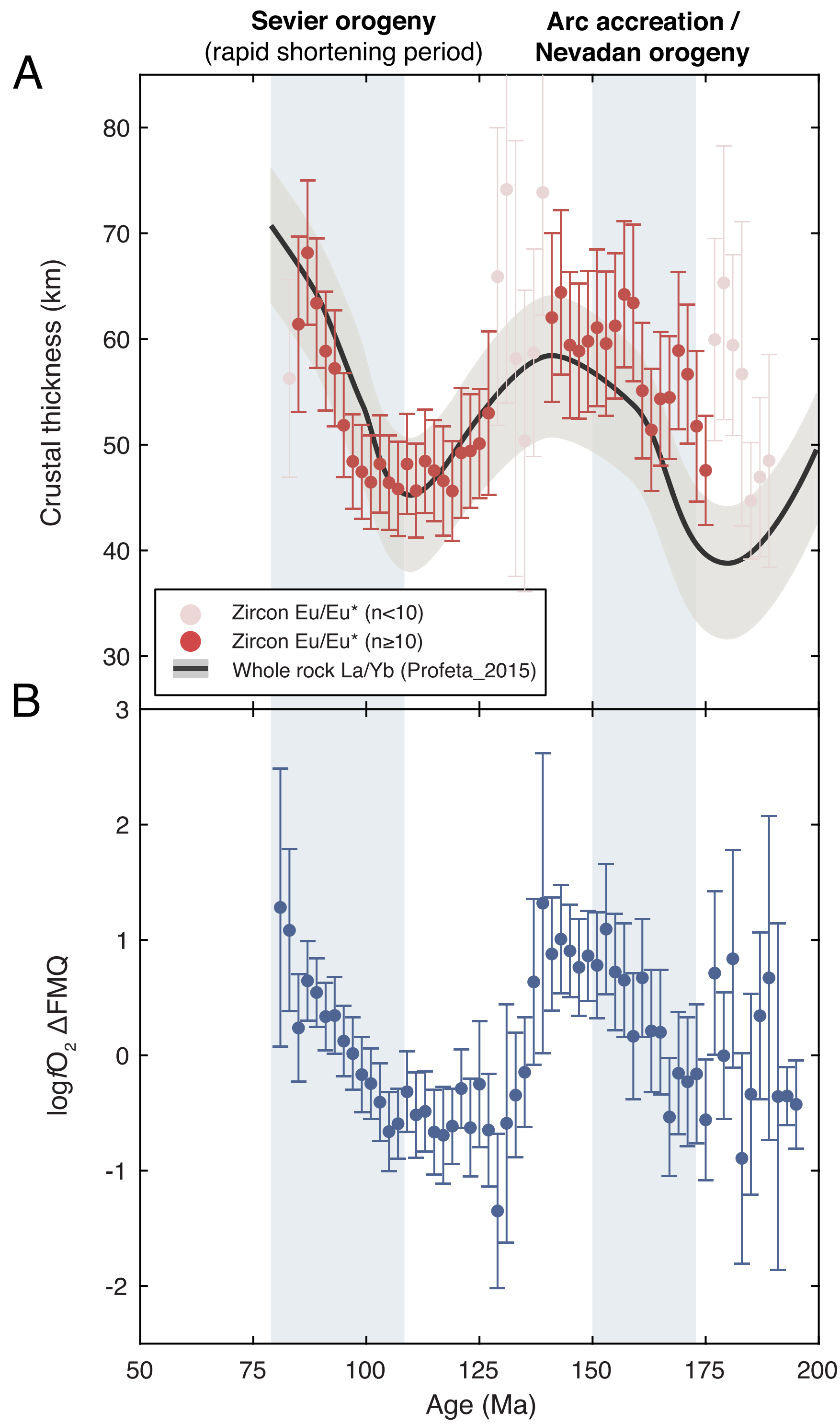

Fig. 4. Comparing trends of crustal thickness (A) and fO_2 (B) from the zircon Ce-Ti-U oxybarometer (Loucks et al., 2020) for the Sierra Nevada Batholith. Similar to the crustal thickness data, the fO_2 data are plotted as binned averages (bin size = 2 Myr) and 2 SE errors.

highlights the role of crustal thickness in controlling the oxidation of felsic magmas.

Application of the zircon Ce-Ti-U oxybarometer (Loucks et al., 2020) is not without complexity, though. To remove the influence of magma differentiation, Loucks et al. (2020) assumed a constant slope of d log (Ce/U)/d log(U/Ti) = –0.5 for magma compositions in the formulation of their zircon Ce-Ti-U oxybarometer. This assumption, however, may oversimplify the compositional evolution of magmas differentiating under different crustal thicknesses (Tang et al., 2024a). How this assumption may impact the calculated fO_2 may be further evaluated by future work.

5.2.2. *Magma water content*

Magma water content strongly controls plagioclase crystallization with high water content suppressing plagioclase saturation (Almeev et al., 2012; Botcharnikov et al., 2008). Interestingly, similar to redox conditions, magma water content has also been found to correlate with differentiation pressure. In arcs with thick crusts, where differentiation occurs at greater depths, magmas evolve toward more hydrous compositions than those generated in thinner crust and shallower differentiation depths (Klein et al., 2023). The elevated water content would limit plagioclase fractionation at depth, resulting in higher Eu/Eu* in the melt and subsequently crystallizing zircon.

5.2.3. Differentiation

Because plagioclase crystallization changes Eu/Eu* in the melt constantly, the extent of differentiation has also been considered a variable that would complicate the interpretation of zircon Eu/Eu* data (Yakymchuk et al., 2023). However, the majority of zircon typically crystallize in a narrow temperature range. To achieve zircon saturation at earlier stages of differentiation, higher temperatures would suffice substantially higher Zr concentrations in the melt. For example, In the temperature range of 600–1000°C, each 100°C increase in temperature will result in at least a doubling of the melt Zr concentration to reach zircon saturation (Boehnke et al., 2013). As arc magma differentiates, zircon typically saturates at ~70 wt.% melt SiO_2 content (note that this SiO_2 content should not be confused with that of whole rocks) (Lee and Bachmann, 2014). On the other hand, because Th/U in zircon decreases with decreasing crystalizing temperature (Kirkland et al., 2015; Tang et al., 2014), the Th/U filter, which is used to eliminate zircon of metamorphic origins, would also exclude zircon crystallizing from the most evolved magmas. Together, these factors serve to restrict the impact of differentiation on zircon Eu/Eu*.

Nonetheless, it is worth noting that zircon crystals, even from a single pluton, exhibit a spectrum of Eu/Eu* values. However, this variability, likely caused by continuous plagioclase co-crystallization or redox fluctuation, does not undermine the observation that the ***average*** zircon Eu/Eu* ratio correlates with differentiation pressure and crustal thickness (Tang et al., 2021b). The robustness of this correlation is borne out in the successful reconstructions of crustal thickness in both the Gangdese belt and Sierra Nevada based on the average Eu/Eu* of detrital zircon. Therefore, we emphasize the importance of a sufficiently large number of zircon analyses to capture the overall distribution, as this is crucial for obtaining a reliable constraint on crustal thickness.

An alternative to averaging large amounts of analyses is to perform differentiation/crystallization correction. This would be the same idea of correcting mid-ocean basalt compositions to 8 wt.% MgO (Klein and Langmuir, 1987). To implement differentiation correction requires robust zircon-based differentiation indices. Zircon Zr/Hf ratio has been proposed as proxy for the degree of differentiation and zircon crystallization (Claiborne et al., 2006; Ibañez-Mejia and Tissot, 2019). However, zircon Eu/Eu* does not show a strong correlation with zircon Zr/Hf in our detrital zircon dataset (Fig. 5), making differentiation correction based on zircon Zr/Hf practically challenging. We suggest that more efforts are needed to fully understand the zircon Zr/Hf-Eu/Eu* systematics. Additionally, redox fluctuations in the shallow magma chamber, although having a secondary influence on the average zircon Eu/Eu*, may further complicate this differentiation correction.

5.2.4. Source composition

The influence of source composition on zircon Eu/Eu* is most evident in S-type granites sourced from metasedimentary rocks (Tang et al., 2021b; Yakymchuk et al., 2023). These metasedimentary rocks are derived from upper crustal terrigenous materials, and may inherit the low and heterogenous Eu/Eu* ratios of the upper continental crust (Rudnick and Gao, 2014). Furthermore, the organic carbon from sediments are progressively metamorphosed to graphite that may lead to reduced melts during anatexis (e.g., Flood and Shaw, 1975). The low Eu/Eu* protoliths and reduced compositions would together result in low Eu/Eu* in zircon crystallizing from S-type granites, which has been shown by Tang et al. (2021b). Furthermore, S-type granitic magmas typically fractionate in the upper crust. Hence, Eu/Eu* in S-type zircon cannot be used to calculate crustal thickness and the zircon dataset must be filtered for S-type zircon grains using robust indicators.

Burnham and Berry (2017) and Zhu et al. (2020) identified high P concentrations in zircon as indicative of S-type granite origin. More recently, this argument was challenged by Bucholz et al. (2022), who showed that zircon grains from Precambrian S-type granites (or strongly peraluminous granites) do not necessarily exhibit high P concentrations. This discrepancy is attributed to their parental melts having lower P concentrations than Phanerozoic equivalents. Therefore, while P concentration may remain a useful criterion for identifying S-type zircon of Phanerozoic ages, a more robust indicator is required for identifying S-type zircon in the Precambrian. One such candidate could be zircon Al concentration (Trail et al., 2017), offering a more robust method for identifying S-type zircons in Precambrian context.

While basalts have distinct and more uniform compositions compared with sedimentary rocks, Triantafyllou et al. (2023) showed that even a small compositional variability in basaltic protoliths can impact phase equilibria during partial melting and lead to substantial changes in zircon Eu/Eu*. This sensitivity to basalt major element compositions would also affect the La/Yb and Sr/Y proxies for crustal thickness. However, the La/Yb and Sr/Y proxies have been extensively utilized and, in most cases, have provided reasonable constraints on crustal thickness for a series of magmatic orogens (e.g., Chapman et al.,

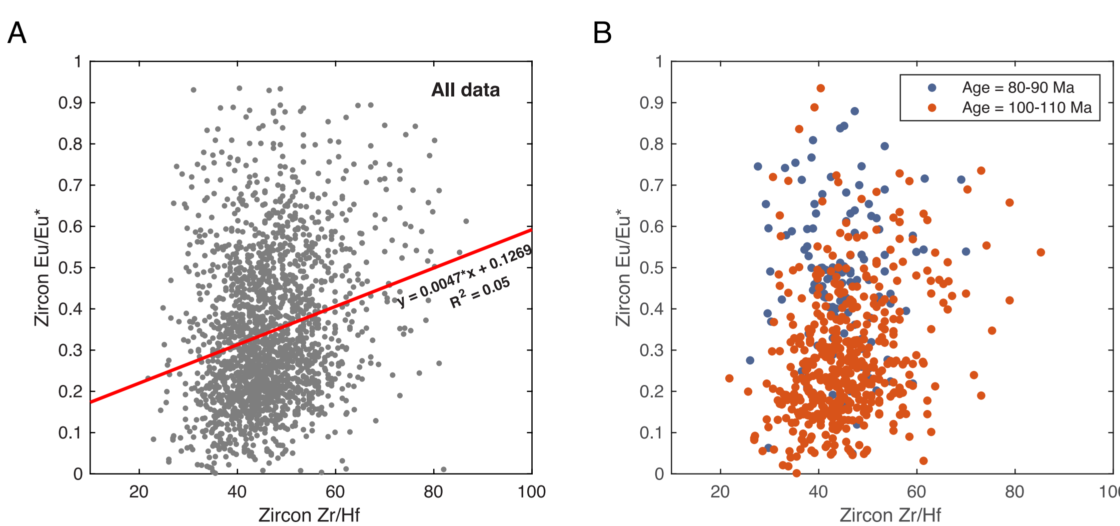

Fig. 5. Zircon Eu/Eu*-Zr/Hf relationships in our Sierran Nevada detrital zircon dataset. A. All data are plotted. B. Two subsets of data with ages of 80–90 Ma and 100–110 Ma are plotted.

2015; Chapman et al., 2020; Farner and Lee, 2017; Zhu et al., 2017).

We note that the phase equilibria modeling by Triantafyllou et al. (2023) hinges critically on several assumptions and simplifications. Key among these is the use of activity model for silicate melt (Green et al., 2016), which could result in unexpected melting behaviors of metabasites (e.g., Johnson et al., 2017). Furthermore, the model by Triantafyllou et al. (2023) potentially underestimates the stability of garnet by excluding Mn from its model system, thereby diminishing the role of garnet fractionation in comparison to what is observed in natural settings. Moreover, these models were built upon thermodynamic parameters obtained from experimental and natural assemblages. When there is a divergence between modeling outcomes and empirical observations, it necessitates additional calibration of thermodynamic and partitioning models to resolve these discrepancies.

5.3. Models vs. observations—what is missing?

The studies of the Sierra Nevada and Gangdese Batholiths lend support to zircon Eu/Eu* as a robust proxy for reconstructing crustal thickness evolution in magmatic orogens. These observations stand in contrast to the conclusions of studies based on phase equilibria and geochemical modeling (Triantafyllou et al., 2023; Yakymchuk et al., 2023). What insights, then, can we learn from these modeling endeavors? Undoubtedly, these approaches are useful for defining phase relationships and chemical evolution in anatexis. In the case of zircon Eu/Eu*, these efforts offer complementary insights into the underlying complexities and potential limitations of this proxy. However, it is essential to recognize that these modeling experiments are typically designed following the **reductionist approach**, where variables are isolated and examined individually. Relying solely on these models may lead to overlooking the systematic interactions and the resultant new properties. This limitation is evident in the connections between crustal thickness, differentiation pressure, magma water content, and redox condition (Fig. 6). These underlying connections are integral to understanding the complex dynamics at play in magmatic and metamorphic processes. To fully grasp these complexities and interconnections, it is essential to consider **systems thinking approaches** in formulating future models.

5.4. Limitations of the zircon Eu/Eu proxy*

Zircon Eu/Eu* exhibits intrinsic variability due to factors such as plagioclase co-crystallization and local fluctuation in redox conditions within the magma chamber. The efficacy of zircon Eu/Eu* as a proxy for crustal thickness is realized only when a large number of analyses are available to mitigate the impacts of random sampling of heterogeneous populations—a fundamental principle behind big data analysis. This same logic holds true for using whole-rock La/Yb ratio to reconstruct crustal thickness. For this reason, a single zircon Eu/Eu* analysis bears no direct insights into differentiation pressure or crustal thickness—an important consideration acknowledged by Tang et al. (2021b) and corroborated by recent petrologic modeling studies (Triantafyllou et al., 2023; Yakymchuk et al., 2023).

At the scale of individual plutons or volcanoes, average zircon Eu/Eu* can potentially be used to calculate local crustal thickness, but the interpretation may become intricate due to spatially or temporarily heterogeneous sources or differentiation processes. This complexity at the pluton/volcano scale is also seen in whole-rock La/Yb ratios. While at the scale of arc segments, average magma La/Yb ratios show a strong correlation with crustal thickness, individual plutons/volcanos usually display significant variations in average magma La/Yb ratios (Farner and Lee, 2017).

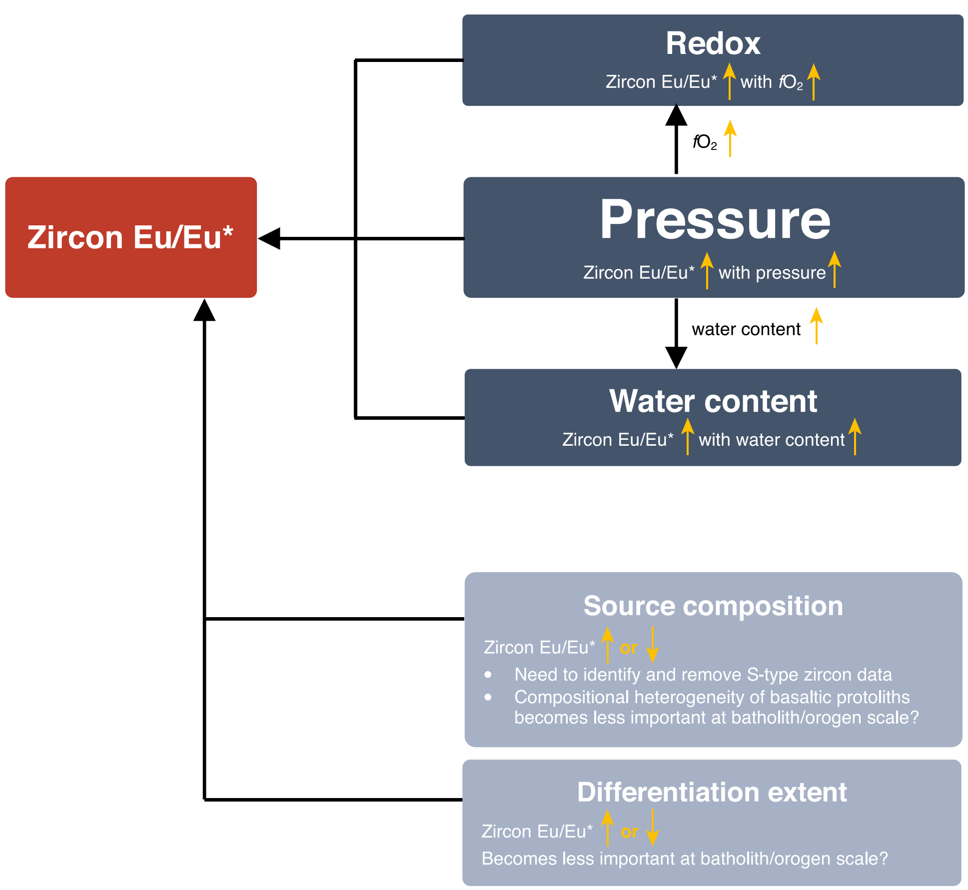

Fig. 6. Chart explaining the major factors that may impact zircon Eu/Eu* and the interconnections between these factors.

The zircon Eu/Eu* proxy is most effective when applied to extensive detrital zircon from a variety of sources to constrain average crustal thickness evolution at the batholith or orogen scale. At this broader scale, the effects of heterogeneous sources and differentiation processes on zircon Eu/Eu* (and whole-rock La/Yb) are minimized, and the influence of differentiation pressure/crustal thickness on average zircon Eu/Eu* become first order.

We concur with Triantafyllou et al. (2023) that extending the application of zircon Eu/Eu* proxy to Earth's deep time can be a bold endeavor. The primary uncertainty lies in the secular evolution in the composition of protoliths for felsic magmas, and whether this source evolution may impact the average zircon Eu/Eu* on the first order. Further insights to these questions may be gained through future models that comprehensively consider the interplay between magma differentiation pressure, water content, redox condition, plagioclase co-crystallization, and source composition, and the interconnections among these factors.

6. Conclusions

Application of the zircon Eu/Eu* proxy to the detrital zircon in the Sierra Nevada batholith yields a crustal thickness evolution pattern that is consistent with findings from whole-rock La/Yb data and other geological observations.

Zircon Eu/Eu* reflects combined effects of magma differentiation pressure, redox condition, water content, differentiation, and source composition, many of which are interconnected with pressure and enhance the influence of differentiation pressure on zircon Eu/Eu*. Models that emphasize the complexity induced by magma redox condition and water content did not realize these intrinsic interconnections.

The zircon Eu/Eu* proxy is best applied to detrital zircon to constrain average crustal thickness evolution at the batholith or orogen scale. At this scale, differentiation pressure and its associated processes exert the first order control on average zircon Eu/Eu*, whereas the influences of differentiation extent and source heterogeneity become secondary.

Zircon Eu/Eu* remains a valuable proxy for reconstructing crustal thickness with sufficient data analysis and careful data processing and interpretation.

CRediT authorship contribution statement

Ming Tang: Writing – original draft, Visualization, Resources, Methodology, Investigation, Funding acquisition, Formal analysis, Data curation, Conceptualization. **Ziyi Guo:** Visualization, Data curation. **Wenrong Cao:** Writing – review & editing, Resources, Investigation. **Xu Chu:** Writing – review & editing, Investigation.

Declaration of competing interest

The authors declare that they have no known competing financial interests or personal relationships that could have appeared to influence the work reported in this paper.

Data availability

Data will be made available on request.

Acknowledgments

We thank Emily J. Chin, one anonymous reviewer, and Editor Fangzhen Teng for their constructive comments. We also thank Scott McCoy and Sophie Rothman for providing river sand samples from San Joaquin, Kings, and Kawean Rivers. Jeremy Wu and Xincheng Zhou are thanked for helping with sample collection. This work was financially supported by National Natural Science Foundation of China (grants 42125302, 42073026, and 41888101). M.T. is grateful for the support from the New Cornerstone Science Foundation through the XPLORER PRIZE.

Supplementary materials

Supplementary material associated with this article can be found, in the online version, at doi:10.1016/j.epsl.2024.118897.

References

Almeev, R.R., Holtz, F., Koepke, J., Parat, F., 2012. Experimental calibration of the effect of H2O on plagioclase crystallization in basaltic melt at 200 MPa. Am. Mineralog. 97, 1234–1240.

Attia, S., Paterson, S.R., Saleeby, J., Cao, W., 2021. Detrital zircon provenance and depositional links of Mesozoic Sierra Nevada intra-arc strata. Geosphere 17, 1422–1453.

Boehnke, P., Watson, E.B., Trail, D., Harrison, T.M., Schmitt, A.K., 2013. Zircon saturation re-revisited. Chem. Geol. 351, 324–334.

Botcharnikov, R., Almeev, R., Koepke, J., Holtz, F., 2008. Phase relations and liquid lines of descent in hydrous ferrobasalt—implications for the Skaergaard intrusion and Columbia River flood basalts. J. Petrol. 49, 1687–1727.

Brudner, A., Jiang, H., Chu, X., Tang, M., 2022. Crustal thickness of the Grenville orogen: A Mesoproterozoic Tibet? Geology 50, 402–406.

Bucholz, C., Liebmann, J., Spencer, C., 2022. Secular variability in zircon phosphorus concentrations prevents simple petrogenetic classification. Geochem. Perspect. Lett. 24, 12–16.

Burnham, A.D., Berry, A.J., 2012. An experimental study of trace element partitioning between zircon and melt as a function of oxygen fugacity. Geochim. Cosmochim. Acta 95, 196–212.

Burnham, A.D., Berry, A.J., 2017. Formation of Hadean granites by melting of igneous crust. Nat. Geosci. 10, 457–461.

Busby-Spera, C.J., 1988. Speculative tectonic model for the early Mesozoic arc of the southwest Cordilleran United States. Geology 16, 1121–1125.

Cao, W., Bataille, C.P., Leuchter, E.R., Zhou, X., 2022. Tectonic controls on the isotopic juvenility of mid-Cretaceous continental arcs: Global compilations and implications for chemical weathering. Earth Planet. Sci. Lett. 587, 117550.

Cao, W., Paterson, S., 2016. A mass balance and isostasy model: Exploring the interplay between magmatism, deformation and surface erosion in continental arcs using central Sierra Nevada as a case study. Geochem. Geophys. Geosyst. 17, 2194–2212.

Cao, W., Paterson, S., Memeti, V., Mundil, R., Anderson, J.L., Schmidt, K., 2015. Tracking paleodeformation fields in the Mesozoic central Sierra Nevada arc: Implications for intra-arc cyclic deformation and arc tempos. Lithosphere 7, 296–320.

Cao, W., Paterson, S., Saleeby, J., Zalunardo, S., 2016. Bulk arc strain, crustal thickening, magma emplacement, and mass balances in the Mesozoic Sierra Nevada arc. J. Struct. Geol. 84, 14–30.

Chapman, J.B., Ducea, M.N., DeCelles, P.G., Profeta, L., 2015. Tracking changes in crustal thickness during orogenic evolution with Sr/Y: An example from the North American Cordillera. Geology 43, 919–922.

Chapman, J.B., Greig, R., Haxel, G.B., 2020. Geochemical evidence for an orogenic plateau in the southern US and northern Mexican Cordillera during the Laramide orogeny. Geology 48, 164–168.

Chen, K., Tang, M., Hu, Z., Liu, Y., 2023. Generation of tholeiitic and calc-alkaline arc magmas and its implications for continental growth. Geochim. Cosmochim. Acta 355, 173–183.

Chen, Y., Meng, J., Liu, H., Wang, C., Tang, M., Liu, T., Zhao, Y., 2022. Detrital zircons record the evolution of the Cathaysian Coastal Mountains along the South China margin. Basin Res. 34, 688–701.

Chiaradia, M., 2015. Crustal thickness control on Sr/Y signatures of recent arc magmas: an Earth scale perspective. Scientif. Rep. 5.

Chin, E., Lee, C., Blichert-Toft, J., 2015. Growth of upper plate lithosphere controls tempo of arc magmatism: Constraints from Al-diffusion kinetics and coupled Lu-Hf and Sm-Nd chronology. Geochem. Perspect. Lett. 1, 20–32.

Chin, E.J., Lee, C.-T.A., Tollstrup, D.L., Xie, L., Wimpenny, J.B., Yin, Q.-Z., 2013. On the origin of hot metasedimentary quartzites in the lower crust of continental arcs. Earth Planet. Sci. Lett. 361, 120–133.

Claiborne, L.L., Miller, C., Walker, B., Wooden, J., Mazdab, F., Bea, F., 2006. Tracking magmatic processes through Zr/Hf ratios in rocks and Hf and Ti zoning in zircons: an example from the Spirit Mountain batholith, Nevada. Mineralog. Magaz. 70, 517–543.

DeCelles, P.G., 2004. Late Jurassic to Eocene evolution of the Cordilleran thrust belt and foreland basin system, western USA. Am. J. Sci. 304, 105–168.

DeCelles, P.G., Ducea, M.N., Kapp, P., Zandt, G., 2009. Cyclicity in Cordilleran orogenic systems. Nat. Geosci. 2, 251–257.

Dickinson, W.R., 2004. Evolution of the North American cordillera. Ann. Rev. Earth Planet. Sci. 32, 13–45.

Ducea, M., Saleeby, J., 1998a. A case for delamination of the deep batholithic crust beneath the Sierra Nevada, California. Int. Geol. Rev. 40, 78–93.

Ducea, M.N., Saleeby, J.B., 1998b. The age and origin of a thick mafic–ultramafic keel from beneath the Sierra Nevada batholith. Contribut. Mineral. Petrol. 133, 169–185.

Farner, M.J., Lee, C.-T.A., 2017. Effects of crustal thickness on magmatic differentiation in subduction zone volcanism: A global study. Earth Planet. Sci. Lett. 470, 96–107.
Flood, R., Shaw, S., 1975. A cordierite-bearing granite suite from the New England Batholith, NSW, Australia. Contribut. Mineral. Petrol. 52, 157–164.
Goltz, A.E., Krawczynski, M.J., McCanta, M.C., Darby Dyar, M., 2022. Experimental calibration of an Fe3+/Fe2+-in-amphibole oxybarometer and its application to shallow magmatic processes at Shiveluch Volcano, Kamchatka. Am. Mineralog. 107, 2084–2100.
Green, E.C.R., White, R.W., Diener, J.F.A., Powell, R., Holland, T.J.B., Palin, R.M., 2016. Activity–composition relations for the calculation of partial melting equilibria in metabasic rocks. J. Metamorph. Geol. 34, 845–869.
Green, T., 1982. Anatexis of Mafic Crust and High Pressure Crystallization of Andesite. American Society of Mechanical Engineers (Paper), pp. 465–487.
Haschke, M., Scheuber, E., Günther, A., Reutter, K.J., 2002. Evolutionary cycles during the Andean orogeny: repeated slab breakoff and flat subduction? Terra Nova 14, 49–55.
Holycross, M., Cottrell, E., 2023. Garnet crystallization does not drive oxidation at arcs. Science 380, 506–509.
Hoskin, P.W., Schaltegger, U., 2003. The composition of zircon and igneous and metamorphic petrogenesis. Rev. Mineral. Geochem. 53, 27–62.
Huang, C., Wang, H., Yang, J.H., Ramezani, J., Yang, C., Zhang, S.B., Yang, Y.H., Xia, X. P., Feng, L.J., Lin, J., 2019. SA01–A proposed Zircon reference material for microbeam U-Pb Age and Hf-O isotopic determination. Geostand. Geoanalyt. Res.
Ibañez-Mejia, M., Tissot, F.L., 2019. Extreme Zr stable isotope fractionation during magmatic fractional crystallization. Sci. Adv. 5, eaax8648.
Ji, W.-Q., Wu, F.-Y., Wang, J.-M., Liu, X.-C., Liu, Z.-C., Zhang, Z., Cao, W., Wang, J.-G., Zhang, C., 2020. Early evolution of himalayan orogenic belt and generation of middle eocene magmatism: constraint from Haweng Granodiorite Porphyry in the Tethyan Himalaya. Front. Earth Sci. 8.
Johnson, T.E., Brown, M., Gardiner, N.J., Kirkland, C.L., Smithies, R.H., 2017. Earth's first stable continents did not form by subduction. Nature 543, 239–242.
Kirkland, C.L., Smithies, R.H., Taylor, R.J.M., Evans, N., McDonald, B., 2015. Zircon Th/U ratios in magmatic environs. Lithos 212-215, 397–414.
Klein, B.Z., Jagoutz, O., Schmidt, M.W., Kueter, N., 2023. A global assessment of the controls on the fractionation of arc magmas. Geochem. Geophys. Geosyst. 24, e2023GC010888.
Klein, E.M., Langmuir, C.H., 1987. Global correlations of ocean ridge basalt chemistry with axial depth and crustal thickness. J. Geophys. Res.: Solid Earth 92, 8089–8115.
Lee, C.-T.A., Bachmann, O., 2014. How important is the role of crystal fractionation in making intermediate magmas? Insights from Zr and P systematics. Earth Planet. Sci. Lett. 393, 266–274.
Lee, C.-T.A., Thurner, S., Paterson, S., Cao, W., 2015. The rise and fall of continental arcs: Interplays between magmatism, uplift, weathering, and climate. Earth Planet. Sci. Lett. 425, 105–119.
Lewis, M.J., Ryan-Davis, J.R., Bucholz, C.E., 2023. Mafic Intrusions Record Mantle Inputs and Crustal Thickness in the Eastern Sierra Nevada Batholith. Geological Society of America Bulletin, California, USA.
Lieu, W.K., Stern, R.J., 2019. The robustness of Sr/Y and La/Yb as proxies for crust thickness in modern arcs. Geosphere 15, 621–641.
Loader, M.A., Wilkinson, J.J., Armstrong, R.N., 2017. The effect of titanite crystallisation on Eu and Ce anomalies in zircon and its implications for the assessment of porphyry Cu deposit fertility. Earth Planet. Sci. Lett. 472, 107–119.
Loucks, R.R., Fiorentini, M.L., Henríquez, G.J., 2020. New magmatic oxybarometer using trace elements in zircon. J. Petrol. 61, egaa034.
Luo, C.-H., Wang, R., Nebel, O., Li, Q.-W., 2024. Amphibole fractionation as a key driver for oxidation of magmas in convergent margins. Earth Planet. Sci. Lett. 641, 118851.
Paterson, S.R., Ducea, M.N., 2015. Arc magmatic tempos: gathering the evidence. Elements 11, 91–98.
Profeta, L., Ducea, M.N., Chapman, J.B., Paterson, S.R., Gonzales, S.M.H., Kirsch, M., Petrescu, L., DeCelles, P.G., 2015. Quantifying crustal thickness over time in magmatic arcs. Scientif. Rep. 5.
Rapp, R.P., Watson, E.B., 1995. Dehydration melting of metabasalt at 8–32 kbar: implications for continental growth and crust-mantle recycling. J. Petrol. 36, 891–931.
Ren, M., 2004. Partitioning of Sr, Ba, Rb, Y, and LREE between alkali feldspar and peraluminous silicic magma. Am. Mineralog. 89, 1290–1303.
Roberts, N.M.W., Spencer, C.J., Puetz, S., Keller, C.B., Tapster, S., 2024. Regional trends and petrologic factors inhibit global interpretations of zircon trace element compositions. Geosci. Front. 15, 101852.
Rudnick, R.L., Gao, S., 2014. 4.1 - Composition of the Continental Crust. In: Holland, H. D., Turekian, K.K. (Eds.), Treatise on Geochemistry, Second Edition. Elsevier, Oxford, pp. 1–51.
Saleeby, J., Ducea, M., Clemens-Knott, D., 2003. Production and loss of high-density batholithic root, southern Sierra Nevada, California. Tectonics 22.
Saleeby, J., Dunne, G., Anderson, T., Didenko, A., Johnson, C., Khanchuk, A., MacDonald, J., 2015. Temporal and tectonic relations of early Mesozoic arc magmatism, southern Sierra Nevada, California. In: Late Jurassic Margin of Laurasia—A Record of Faulting Accommodating Plate Rotation, 513. Geological Society of America Special Paper, pp. 223–268.
Schweickert, R.A., Anderson, T., Didenko, A., Johnson, C., Khanchuk, A., MacDonald, J., 2015. Jurassic evolution of the Western Sierra Nevada metamorphic province. In: Late Jurassic Margin of Laurasia—A Record of Faulting Accommodating Plate Rotation, 513. Geological Society of America Special Paper, pp. 299–358.
Sun, C., Lee, C.-T.A., 2022. Redox evolution of crystallizing magmas with CHOS volatiles and its implications for atmospheric oxygenation. Geochim. Cosmochim. Acta 338, 302–321.
Sundell, K.E., George, S.W.M., Carrapa, B., Gehrels, G.E., Ducea, M.N., Saylor, J.E., Pepper, M., 2022. Crustal thickening of the Northern Central Andean Plateau inferred from trace elements in Zircon. Geophys. Res. Lett. 49, e2021GL096443.
Tang, M., Chen, H., Song, S., Sun, G., Wang, C., 2024a. Zircon Eu/Eu* in Archean TTGs with implications for the role of endogenic oxidation in Archean crustal differentiation. Geochim. Cosmochim. Acta 378, 259–269.
Tang, M., Chen, H., Song, S., Sun, G., Wang, C., 2024b. Zircon Eu/Eu* in Archean TTGs with implications for the role of endogenic oxidation in Archean crustal differentiation. Geochim. Cosmochim. Acta.
Tang, M., Chu, X., Hao, J., Shen, B., 2021a. Orogenic quiescence in Earth's middle age. Science 371, 728–731.
Tang, M., Erdman, M., Eldridge, G., Lee, C.-T.A., 2018. The redox "filter" beneath magmatic orogens and the formation of continental crust. Sci. Adv. 4.
Tang, M., Ji, W.-Q., Chu, X., Wu, A., Chen, C., 2021b. Reconstructing crustal thickness evolution from europium anomalies in detrital zircons. Geology 49, 76–80.
Tang, M., Lee, C.-T.A., Costin, G., Höfer, H.E., 2019. Recycling reduced iron at the base of magmatic orogens. Earth Planet. Sci. Lett. 528, 115827.
Tang, M., Lee, C.-T.A., Ji, W.-Q., Wang, R., Costin, G., 2020. Crustal thickening and endogenic oxidation of magmatic sulfur. Sci. Adv. 6, eaba6342.
Tang, M., Wang, J., Lee, C.-T.A., 2024c. Reevaluating the oxidation effect of garnet crystallization. Lithos 470-471, 107537.
Tang, M., Wang, X.-L., Shu, X.-J., Wang, D., Yang, T., Gopon, P., 2014. Hafnium isotopic heterogeneity in zircons from granitic rocks: Geochemical evaluation and modeling of "zircon effect" in crustal anatexis. Earth Planet. Sci. Lett. 389, 188–199.
Trail, D., Bruce Watson, E., Tailby, N.D., 2012. Ce and Eu anomalies in zircon as proxies for the oxidation state of magmas. Geochim. Cosmochim. Acta 97, 70–87.
Trail, D., Tailby, N., Wang, Y., Mark Harrison, T., Boehnke, P., 2017. Aluminum in zircon as evidence for peraluminous and metaluminous melts from the Hadean to present. Geochem. Geophys. Geosyst. 18, 1580–1593.
Triantafyllou, A., Ducea, M., Jepson, G., Hernández-Montenegro, J., Bisch, A., Ganne, J., 2023. Europium anomalies in detrital zircons record major transitions in Earth geodynamics at 2.5 Ga and 0.9 Ga. Geology 51 (2), 141–145.
Weill, D.F., Drake, M.J., 1973. Europium Anomaly in Plagioclase Feldspar: Experimental Results and Semiquantitative Model. Science 180, 1059–1060.
Wolf, M.B., Wyllie, P.J., 1993. Garnet growth during amphibolite anatexis: implications of a garnetiferous restite. J. Geol. 101, 357–373.
Yakymchuk, C., Holder, R.M., Kendrick, J., Moyen, J.-F., 2023. Europium anomalies in zircon: A signal of crustal depth? Earth Planet. Sci. Lett. 622, 118405.
Yonkee, W.A., Weil, A.B., 2015. Tectonic evolution of the Sevier and Laramide belts within the North American Cordillera orogenic system. Earth-Sci. Rev. 150, 531–593.
Zhang, J., Wang, R., Hong, J., 2022. Amphibole fractionation and its potential redox effect on arc crust: Evidence from the Kohistan arc cumulates. Am. Mineralog. 107, 1779–1788.
Zhu, D.-C., Wang, Q., Cawood, P.A., Zhao, Z.-D., Mo, X.-X., 2017. Raising the Gangdese Mountains in southern Tibet. J. Geophys. Res.: Solid Earth 122, 214–223.
Zhu, Z., Campbell, I.H., Allen, C.M., Burnham, A.D., 2020. S-type granites: Their origin and distribution through time as determined from detrital zircons. Earth Planet. Sci. Lett. 536, 116140.